

RESEARCH

Open Access



# Numerical analysis of downhole heat exchanger designed for geothermal energy production

I. Akhmadullin\*  and M. Tyagi

\*Correspondence:  
iakhma1@yahoo.com  
Louisiana State University,  
142 Old Forestry Building,  
Baton Rouge, LA 70803, USA

## Abstract

A traditional way of geothermal energy production implies hot brine extraction from the reservoir to a surface facility. This method is economically profitable only for high enthalpy reservoirs associated with shallow depths and high temperatures. The low enthalpy geothermal (LEG) projects are out of consideration due to the high cost of produced electric power related to expensive drilling, cost of the binary cycle system, and long term installation cost. This paper presents a new zero mass extraction method utilizing downhole heat exchanger (DHE) with no geo-fluid production to the surface. The well design stays as a single horizontal well with coupled production and injection sections. The brine pump is located between the sections providing hot brine circulation through the DHE. The coupled fluid flow and heat transfer mathematical model was developed and simulated using nodal analysis method. The LEG reservoir prototype located in South Louisiana was used to study several cases of the DHE lengths, inclination angles, reservoir permeabilities, and flow rates optimization. According to the analysis, the power unit is able to provide 160 kW of net electric power with CO<sub>2</sub> working fluid circulating inside a single lateral well. Increasing the reservoir temperature and the number of laterals, the available power production rises up to 600 kW with an attractive electricity cost of \$21.84/MWh at 7000 m well depth. This methods opens a new prospective for the depleted petroleum wells converting them to the electricity production units.

**Keywords:** Downhole heat exchanger, Low enthalpy geothermal reservoir, Horizontal well, Zero mass extraction method

## Background

Nowadays, geothermal energy production is a well-developed industry where the produced electricity cost is competitive with the traditional fossil fuel power plants. This is true when dealing with high enthalpy reservoirs containing high temperature rock saturated with brine (Kubik 2006). Unfortunately, these resources are few and mostly located at the globe's hot spots. On the other hand, low enthalpy resources (LER) are abandoned but have deep subsurface locations and much lower temperature. For these reasons, LER development requires several complicated and expensive tasks that make the energy production projects economically unprofitable (Lukawski et al. 2014).

The drilling cost varies with the target depth, reservoir rock type, rate of penetration, and a mission of the well. In general, the deep drilling operation may constitute up to 60% of the whole project funds (Lukawski et al. 2014). The geothermal wells usually have larger well diameters, higher rock temperature and pressure, and applied to aggressive geo-fluid causing corrosion and erosion of the well completion (Lukawski et al. 2014; Kubik 2006). That is why the geothermal drilling prices are, usually, higher comparing with conventional oil and gas wells. Additionally to that, a geothermal energy power plant project takes longer time scale from a geological discovery to the power production. All of the above leads to financial failure of the LER projects (Kubik 2006).

One of the possible ways of LER energy production evolution is an application of “zero mass withdrawal method” (ZMW) (Feng 2012; Akhmadullin and Tyagi 2014), which avoids brine extraction to the surface (see Fig. 1). A heat exchanger is installed directly into a hot aquifer where the brine circulation loop is created inside the reservoir. This method allows reducing heat losses from the reservoir, avoiding pipe clogging problems, and reducing a decent portion of a surface area comparing with the traditional binary power plant. This way requires only a single well to complete the power unit, which reduces the construction time.

Literature recognizes the downhole heat exchanger as an advantageous design for heat extraction. Various design ideas of the DHE and formation rock interaction schemes were proposed recently. In general, they can be divided into three groups: conduction,

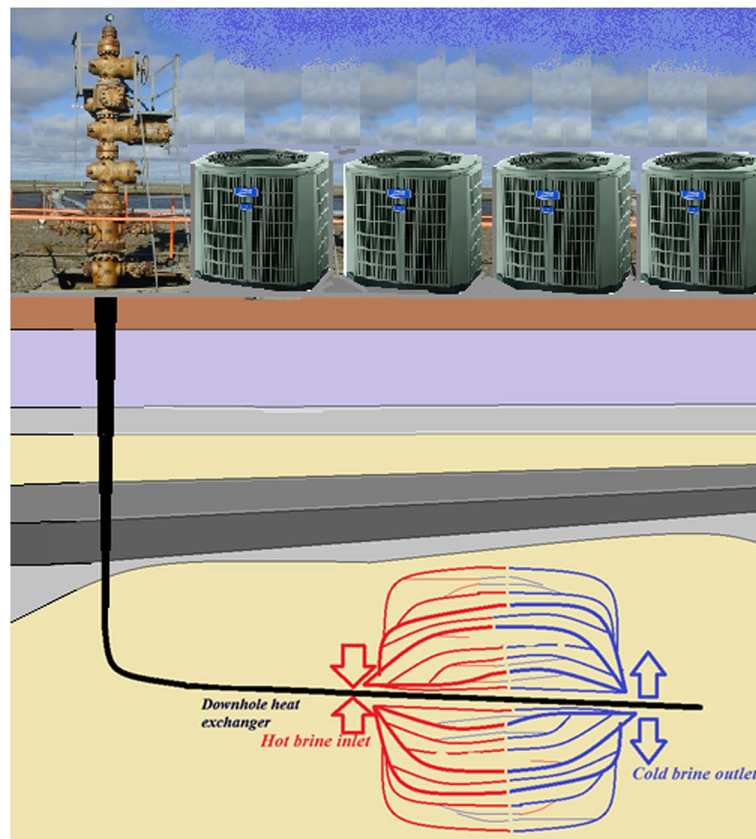


**Fig. 1** Zero mass withdrawal method scheme

natural, and forced convection. A conduction type mostly happens with hot dry rock contact and, practically, is implemented in heat pipe schemes. The power production is commercially unbeneficial due to slow heat exchange process (Nalla et al. 2004). Utilization of a heat transport fluid helps improving heat transfer process. The cheapest case is a hot water brine already existing in the formation. The natural convection type of the DHE/geo-fluid interaction is implemented in the thermosiphon projects (Wang et al. 2009). The design includes a vertical coaxial heat exchanger. The hot brine occupies the outer shell and releases thermal energy to the working fluid moving in the inner tubing. Cooled geo-fluid then enters the reservoir to heat up again and complete a circulation loop. One of the advantages is the absent of a subsurface pump, which is the weakest part of the design due to highly aggressive fluid applications (Dipippo 2008).

The most energy productive method implies forced convection between the DHE and formation fluid. The horizontal orientation of the well inside the reservoir gives an advantage of creating large brine circulation volume without concern of entering cooled brine to the production area (Feng 2012). A pumping equipment is driving brine with an optimal flow range in order to manage heat exchange process and creating enough pumping head to overcome all pressure losses. The maximum pressure drop is expected at the DHE section due to frictional losses associated with exchanger's length. So, the compact DHE is an advantage. From the other side, heat extracted from the reservoir brine is directly proportional to the DHE surface area. Thus, the flow rates and the DHE surface area should be carefully optimized in order to extract maximum heat from the reservoir with the minimum pressure losses.

The problem describing fluid flow in the horizontal pipe with influxes through the porous pipe wall accounts for the energy losses caused by friction, acceleration, flow direction change, and gravity. These values depend on fluid flow regimes (Ouyang et al. 1997). The inflow rate is not constant along the pipe and decays with the distance from the "hill" (beginning of horizontal section) to the "toe" (end of the horizontal pipe) (Ouyang et al. 1997; Anklam 2005; Cho and Shah 2001). This effect is a well-known problem in the petroleum industry, which reduces the productivity of the well (Cho and Shah 2001). Anklam (2005) proved that pressure in the well increases along the pipe moving from the hill to the toe region, and the influx flow rate decreases in the same direction. Ouyang et al. (1997) experimentally explored pressure losses in the perforated pipe at several cases. Frictional losses were the most valuable at high flow rates inside the long well, whereas, accelerational and directional losses were almost negligible.

The influx into the horizontal well can be equalized along the well using influx control devices (ICD) available from the petroleum industry applications (Aadnoy and Hareland 2009). The ICD is a passive flow rate restriction used an additional permanent pressure drop per unit well length (Al-Khelaiwi et al. 2008; Joshi 1988). In this paper, the authors are interested in the effect of the equal influx on the DHE application ignoring particular ICD design.

The purpose of this analysis is to define the optimal DHE length and corresponding working fluid and brine flow rates keeping the net power at the maximum value. The economic analysis determined the competitiveness of the project based on levelized cost of electric power (LCOE) parameter (Walraven et al. 2015). The geopressured reservoir located in Vermilion Parish, Louisiana, US was taken as a reservoir prototype (Gray

2010) and CO<sub>2</sub> was chosen as a working fluid for the power cycle (Sarkar 2015). Reservoir temperature of 126 °C was used in the calculations.

### Methodology

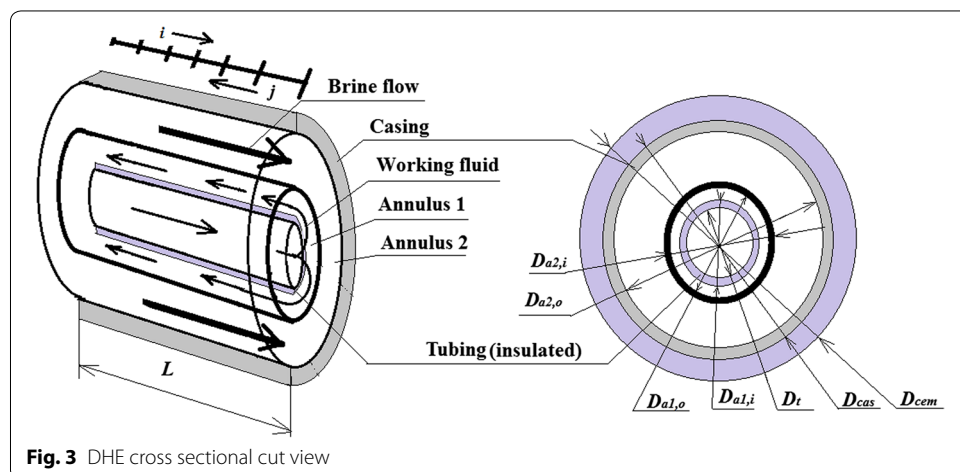
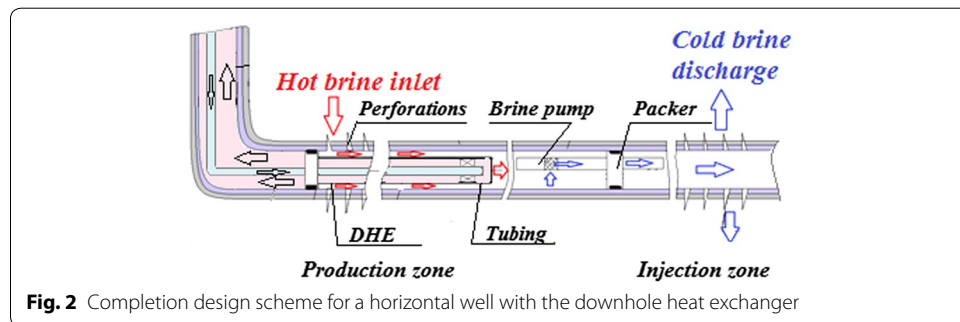
#### Proposed design

The general well scheme is shown in the Fig. 1. The horizontal well design is completed by coupling the production and injection sides by a pump assembly in between as shown in Fig. 2. The production side contains coaxial heat exchanger inside and a gravel pack to protect DHE from erosion. The injection side is located at some interval to prevent cold flow entering the intake region. According to Feng (2012), the distance of 2000 ft is the most beneficial.

Liquid CO<sub>2</sub> is pumped to the DHE from the vertical section through the insulated tubing. At the end of DHE the working fluid flow changes to the opposite direction and travels in the annulus backward (Fig. 3). The brine is penetrated through the perforations in the outer casing annulus and has the opposite flow direction (Feng 2012). The cooled brine is pumped into the injection zone and through the set of perforations leaves the well.

#### Assumptions

The geo-fluid is assumed as an incompressible single phase Newtonian fluid. There is no fluid accumulation inside the pipe. The flow regime is assumed fully developed. The



system operates at a steady state condition. The pressure drawdown area around the well has an elliptical shape (Joshi 1988). The well is performed as a cased and perforated completion to avoid possible burst or collapsing. Perforations are made perpendicular to the horizontal well axis. The perforated intervals are equally distributed along the well. The directions of the working fluid and the brine flow inside the DHE are considered as a counter flow, which is the most efficient for the heat transfer (Feng 2012).

### Net power

To optimize this system, one needs to define the net power produced by the power unit  $\dot{W}_{NET}$ , which is the difference between powers produced by the cycle  $\dot{W}_{cycle}$  and power consumed by the brine pump  $\dot{W}_{b.p.}$ :

$$\dot{W}_{NET} = \dot{W}_{cycle} - \dot{W}_{b.p.} \quad (1)$$

The difference between power produced by the turbine  $\dot{W}_{turb.}$  and losses in the working fluid cooling and pumping equipment  $\dot{W}_{losses}$  define cycle power  $\dot{W}_{cycle}$ :

$$\dot{W}_{cycle} = \dot{W}_{turb.} - \dot{W}_{losses} \quad (2)$$

$\dot{W}_{losses}$  includes working fluid pump power consumption, heat energy losses to the surroundings, and condenser losses, which may consume up to 25% of turbine power:

$$\dot{W}_{cycle} = 0.75\eta_{turb.}\eta_{gen.}\dot{m}_{wf}\Delta H \quad (3)$$

where  $\Delta H$  is the enthalpy difference before and after the turbine stage, which depends on working fluid choice and is a function of working fluid temperature,  $\eta_{turb.}$  and  $\eta_{gen.}$  are efficiencies of turbine and generator,  $\dot{m}_{wf}$  is working fluid mass flow rate.

The project intention is to produce hot reservoir temperature brine for a long operating period. The circular pipe section between production and injection zones was used for separation of cold injection stream from the production zone. The pressure drop was assumed negligible. Combining Eqs. (1), (2), and (3) the net power equation becomes:

$$\dot{W}_{NET} = 0.75\eta_{turb.}\eta_{gen.}\dot{m}_{wf}\Delta H - 2\Delta P_{b.p.}\frac{\dot{m}_b}{\rho_b} \quad (4)$$

where  $\Delta P_{b.p.}$  is a brine pump drawdown pressure,  $\dot{m}_b$  and  $\rho_b$  are mass flow rate and density of the brine.

With rough approximation, let us assume that the working fluid temperature leaving the DHE equal to the turbine inlet temperature ignoring heat losses in the vertical flow (Akhmadullin and Tyagi 2014). Then with constant cold side temperature of 35 °C, the  $\Delta H$  term is easy to define for the chosen fluid. In this project:  $\Delta H = 39.94$  kJ/kg for carbon dioxide. The final working fluid temperature leaving the DHE is fixed with a constant pinch point temperature of 6 °C. Then, the cycle power depends only on working fluid's mass flow rate  $\dot{m}_{wf}$ . The brine pump creates drawdown pressure in the production side and excessive pressure in the injection side as shown in the Fig. 4. The pump pressure head is the sum of these pressures. Assuming that the well completion can be selected in such way that both sides would have the same pressure drop, the pump pressure head is simply two times drawdown pressure  $2\Delta P_{b.p.}$ . The pump drawdown pressure  $2\Delta P_{b.p.}$  is assigned to find every node brine mass flow rate  $\dot{m}_{b(i)}$ .

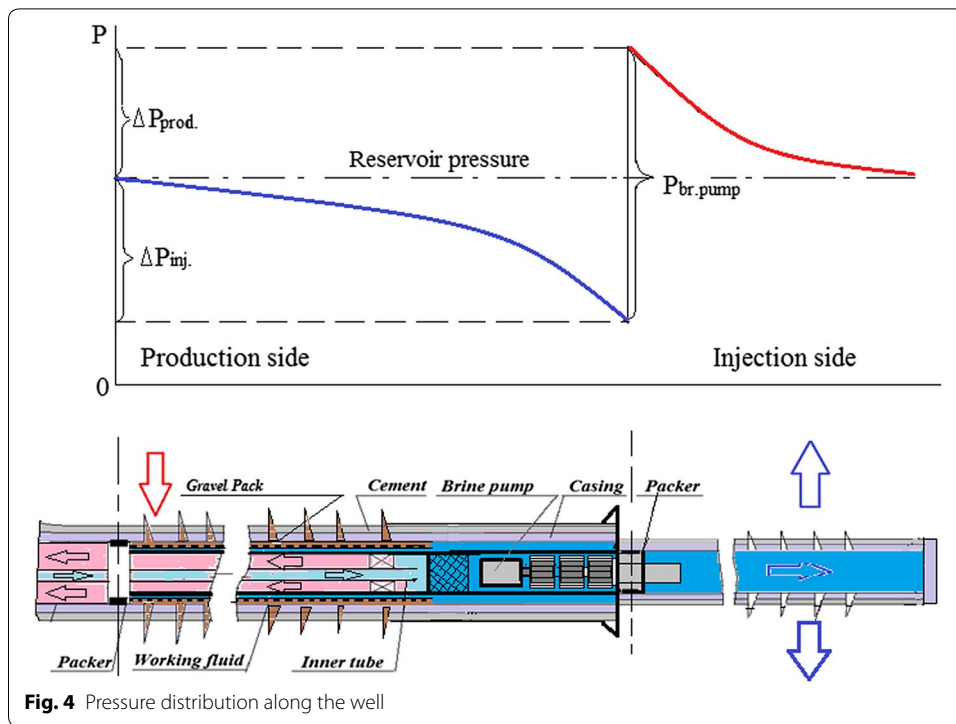


**Fig. 4** Pressure distribution along the well

### Horizontal well nodal analysis

The mathematical system contains several unknown variables: the brine and working fluid flow rates, pump drawdown pressure, and pressure losses at each step of the completion. Let us eliminate some of the parameters to simplify the task. To obtain a pressure distribution model, consider the system which includes the well and the reservoir as shown in Fig. 5. The pressure drops are expected to appear at each part of the system: reservoir, perforations, gravel pack, and ICD. The nodal analysis implies dividing the well length into several intervals and calculating influxes and pressure losses at the each node. Then the total flow rate of the overall production/injection segment is a sum of influxes entering the well. The frictional and gravity pressure drops are expected to make a primary impact on flow rate and pressure development (Ouyang et al. 1997). Therefore, the influx flow rate of each section is a function of the location and is defined by the well flowing pressure at the node.

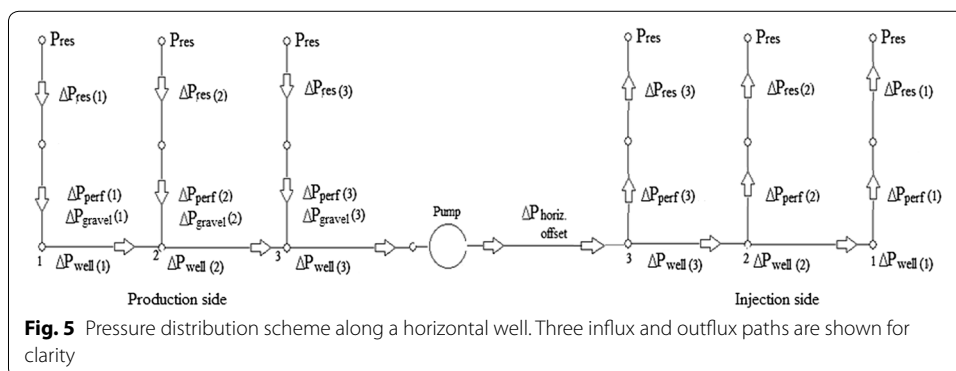


**Fig. 5** Pressure distribution scheme along a horizontal well. Three influx and outflux paths are shown for clarity

According to the mass conservation law, the total flow into the horizontal well is defined by the sum of the reservoir  $i$ -th node flows:

$$Q_{\text{tot}} = \sum_{i=1}^n Q_{(i)} \tag{5}$$

The well flowing pressure of each node is a conceptual pressure at which the influx for the interval is calculated. The nodes numeration starts  $i = 1 \dots n$  for the injection side and  $i = n \dots 1$  for the production side. The  $i = n$  node corresponds to the “toe” of the well for the production side (Fig. 5). The difference between the reservoir  $P_e$  and the well flowing pressure at each node  $P_{\text{well}(i)}$  is a sum of losses in the perforations, gravel pack, and rock porous media.

$$\Delta P_{(i)} = P_e - P_{\text{well}(i)} \tag{6}$$

where the pressure  $\Delta P_{(i)}$  is a sum of pressure resistances in the reservoir  $\Delta P_{\text{res}}$  and a gravel pack  $\Delta P_{\text{gravel}}$ :

$$\Delta P_{(i)} = \Delta P_{\text{res}(i)} + \Delta P_{\text{gravel}(i)} + \Delta P_{\text{perf.}(i)} \tag{7}$$

The description of each term of the Eq. (7) is given in the [Appendix A](#). Let us equate the right hand sides of the Eqs. (6) and (7). Each pressure term can be represented as a multiplication of corresponding flow resistance and the volumetric flow rate  $Q_{\text{in}(i)}$ .

$$P_e - P_{\text{well}(i)} = \Delta P_{\text{res}(i)} + \Delta P_{\text{gravel}(i)} + \Delta P_{\text{perf.}(i)} \tag{8}$$

From the other side, the same pressure drop between the nodes is defined in terms of friction  $F$ , acceleration  $Ac$ , direction  $Dr$ , and gravity  $G$  components of pressure losses inside the well. The friction factor is defined by Ouyang et al. (1997). The gravity term is positive with the assumption of a negative slope well inclination from the horizontal axis.

$$P_{\text{well}(i)} - P_{\text{well}(i-1)} = F_{(i)} Q_{\text{tot}}^2 + Ac_{(i)} Q_{(i)} + Dr_{(i)} Q_{\text{in}(i)}^2 - G_{(i)} \tag{9}$$

where  $a$  and  $b$  are flow resistances (non-Darcy and Darcy terms) of gravel pack pressure drop (Bourgoyne et al. 1986). The gravel pack is assumed as a 20/40 mesh sand with 135 D permeability according to the Weatherford catalog. To eliminate the unknown well flowing pressure term let us add Eqs. (8) and (9):

$$P_e - P_{\text{well}(i-1)} = a_{(i)} Q_{\text{in}(i)}^2 + b_{(i)} Q_{\text{in}(i)} + F_{(i)} Q_{\text{tot}}^2 + Ac_{(i)} Q_{(i)} + Dr_{(i)} Q_{(i)}^2 - G_{(i)} \tag{10}$$

The description of each term in the Eqs. (10) is given in the [Appendix B](#). Adding pressure drops from the previous steps Eq. (9) to the Eq. (10) it is possible to eliminate the well flowing pressures at each node and finally receive pump suction pressure. Then  $\Delta P_{\text{b.p.}} = P_e - P_{\text{well}(n)}$ . The other ( $\Delta P_{\text{b.p.}}$ ) is defined from the injection side. Finally, the quadratic Eq. (10) contains only one unknown  $Q_{(i)}$  and solving it with a positive root:

$$Q_{(i)} = \frac{-B + \sqrt{B^2 - 4AC}}{2A} \tag{11}$$

where

$$A = a_{(i)} + Dr_{(i)} \tag{12}$$

$$B = \Delta P_{\text{perf}(i)} + b_{(i)} + Ac_{(i)} \tag{13}$$

$$C = F_{(i)}Q_{\text{tot}}^2 - (P_e - P_{\text{well}(i-1)}) - G \tag{14}$$

The algorithm based on Eqs. (10) and (11) gives the system of equations equal to the number of nodes. The components are shown in Table 1 for three nodes for demonstration purposes. The system is solved simultaneously with the check point Eq. (5). At the last node, the acceleration pressure drop is equal to zero. The obtained influxes then were converted to the mass flow rates using corresponding brine densities for the nodes:

$$\dot{m}_{(i)} = Q_{(i)}\rho_{(i)} \tag{15}$$

### Heat transfer model

The heat transfer model contains the same number of equations for each node. Two sets of equations were formulated for the brine and working fluid temperatures (Feng 2012). Annuluses 1 and 2 in Fig. 3 represent heat interaction boundaries of two independent loops: brine and working fluid. Brine is engulfed through the perforations into annulus 2. Heat is transferred to the cold working fluid through the pipe thickness. The inner tubing is insulated. The overall heat transfer coefficient is calculated at each node. The formulation is shown in the Appendix C.

### Simulation algorithm

The algorithm is presented in Fig. 6. For the given DHE geometry (Table 2) and reservoir properties (Table 3), the total brine influx and the working fluid mass flow rate was assumed. The new mass flow rates are defined by solving the system of equations shown in Table 1.

The next step was a check point in order to satisfy the error of 1% between the assumed and obtained values. If the error was high, the iteration continued with the new flow rate values. As soon as the brine flow rates at the each node were calculated, the heat transfer was analyzed. The sum of computed heat resistances defined the overall heat transfer coefficient and temperatures. The check point was a pinch point temperature at the DHE, which is a difference between reservoir temperature and working fluid temperature leaving the exchanger. The realistic 6 °C was assumed for this design.

**Table 1 Coefficients of the Eq. (10) for three interval case production side**

Node	A	B	C
1	$a_1 + Dr_1$	$R_{\text{perf}1} + b_1$	$F_1(Q_{\text{tot}} - Q_3 - Q_2)^2 + F_2(Q_{\text{tot}} - Q_3)^2 + F_3(Q_{\text{tot}})^2 + Ac_2Q_2 + Ac_3Q_3 + Dr_2Q_2^2 + Dr_3Q_3^2 - 3G - (P_e - P_{\text{well}(3)})$
2	$a_2 + Dr_2$	$R_{\text{perf}2} + b_2 + Ac_2$	$F_2(Q_{\text{tot}} - Q_3)^2 + F_3(Q_{\text{tot}})^2 + Ac_3Q_3 + Dr_3Q_3^2 - (P_e - P_{\text{well}(3)}) - 2G$
3	$a_3 + Dr_3$	$R_{\text{perf}3} + b_3 + Ac_3$	$F_3(Q_{\text{tot}})^2 - (P_e - P_{\text{well}(3)}) - G$



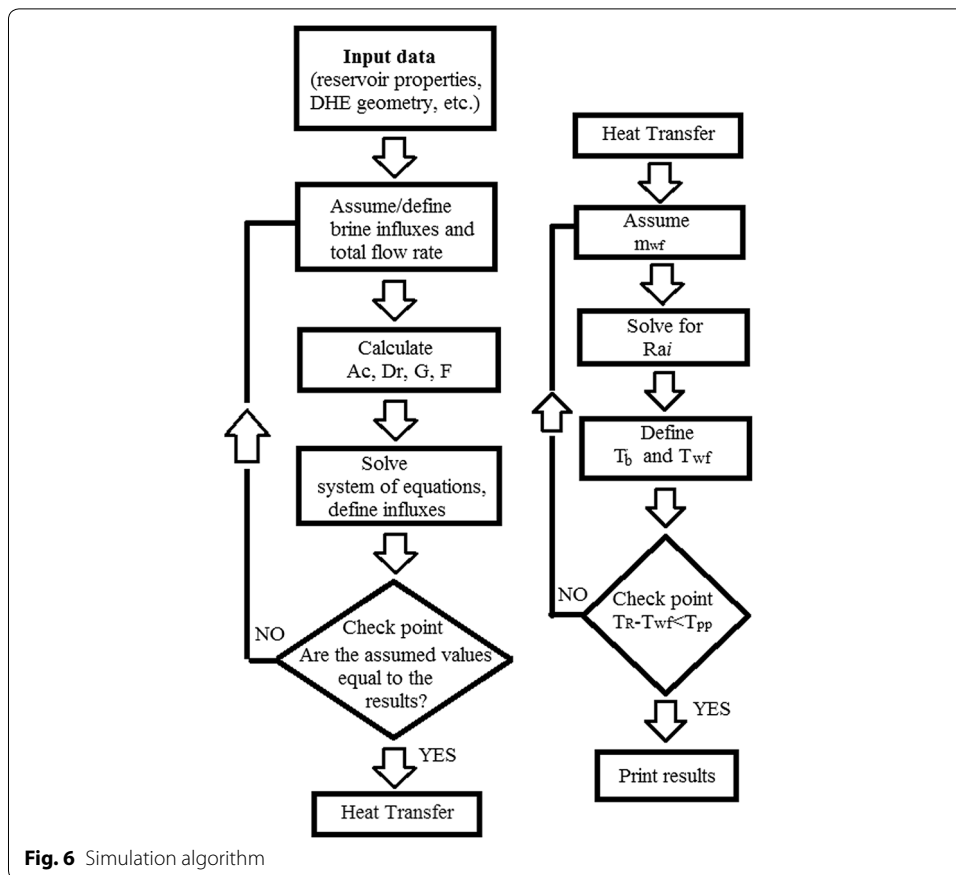


**Table 2** Completion geometry of the well

Cement sheath	
OD	12.527 in. (0.318 m)
Casing 2	
OD	9.625 in. (0.244 m)
ID	8.031 in. (0.204 m)
Screen pipe (gravel pack, ICD)	
OD	6.190 in. (0.157 m)
ID	4.890 in. (0.124 m)
Casing 1 (only production)	
OD	3.5 in. (0.089 m)
ID	2.992 in. (0.076 m)
Tubing (only production)	
OD	1.990 in. (0.051 m)
ID	1.650 in. (0.042 m)

#### Completion design of the injection side

The analysis of the pressure drop inside of the injection section was done in the same manner. There is no DHE, ICD, or gravel pack completion inside the injector pipe. Thus, the outfluxes are expected to be equal at each interval. The total pressure drop at the

**Table 3 Reservoir-prototype characteristics**

Parameter	Value
Permeability (average)	12 mD
Porosity	5–20%
Reservoir pressure	13,015 psi (89.7 MPa)
Reservoir temperature	126 °C
Reservoir thickness	100 m

producer  $\Delta P_{b,p}$  was assigned to the injector. The perforation diameters, and perforated intervals were changed in order to match the pressure drops.

**Input data and validation**

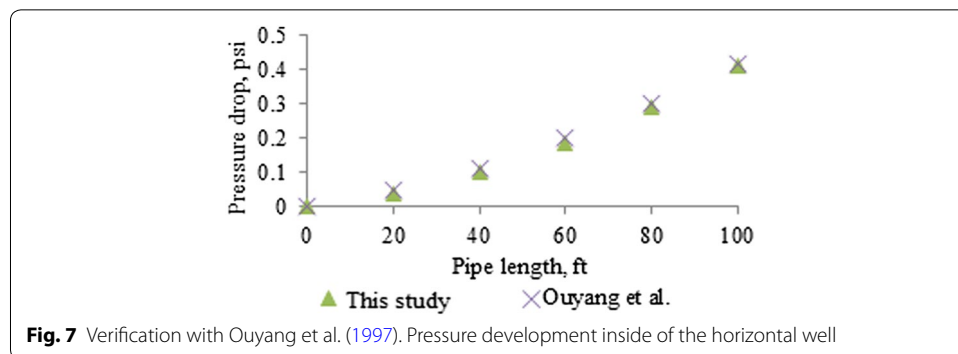
The 0.244 m (9 5/8 in.) casing was chosen for the horizontal well. Reduction of this diameter would lead to increasing frictional pressure losses in the system. Increasing the diameter is hardly possible due to drilling operation procedure, which requires constantly reducing the diameter of the well while reaching the target depth (Bourgoyne et al. 1986).

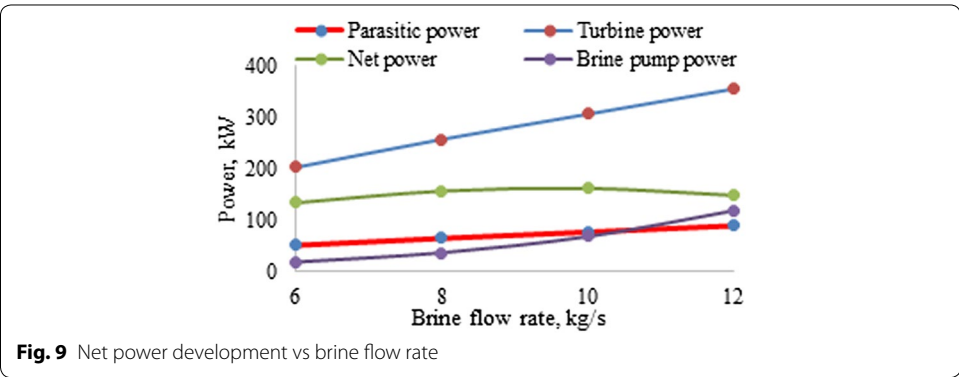
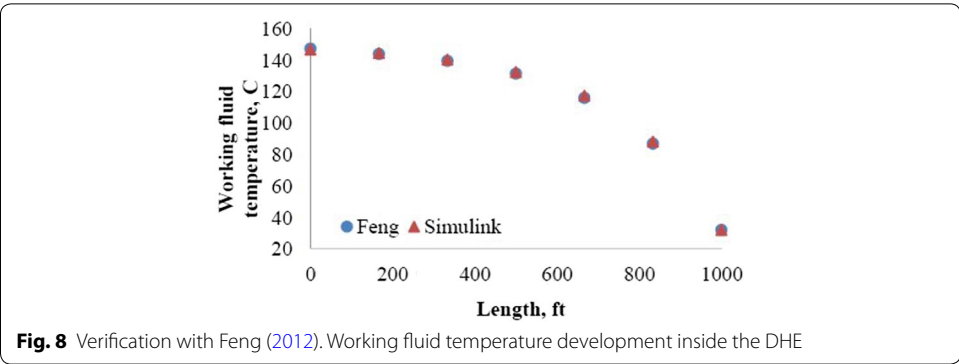
The analysis was performed using Matlab Simulink software. The algorithm was tested with the literature data. First, the horizontal well pressure performance was verified with Ouyang et al. (1997) who experimentally defined pressure distribution along a well. Figure 7 illustrates the comparison of this project code simulation results in terms of pressure development inside of the horizontal well. Then, heat transfer algorithm was tested with *n*-butane working fluid and verified with Feng (2012). Figure 8 shows good match of this project code simulation with the results.

**Results and discussions**

**Net power production**

Figure 9 illustrates simulation results of the net, turbine, brine pump, and parasitic power with the increasing brine flow rate. As it is seen, the net power increases at low brine flow rates, but later reduces due to brine power enhancement associated with frictional losses. The optimal brine flow rate for the given well geometry lies in the range of 8–10 kg/s.

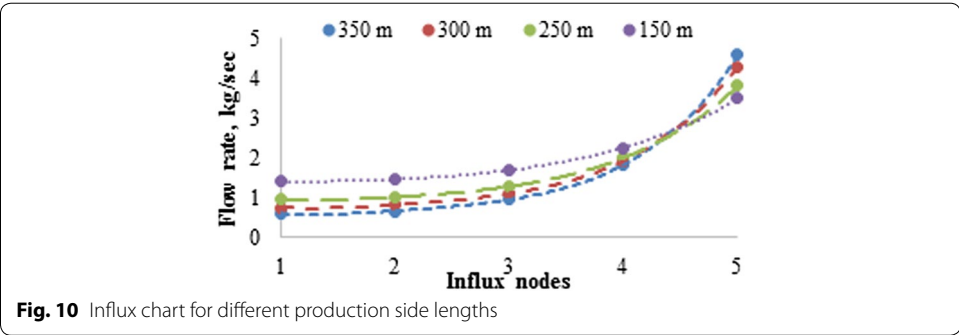


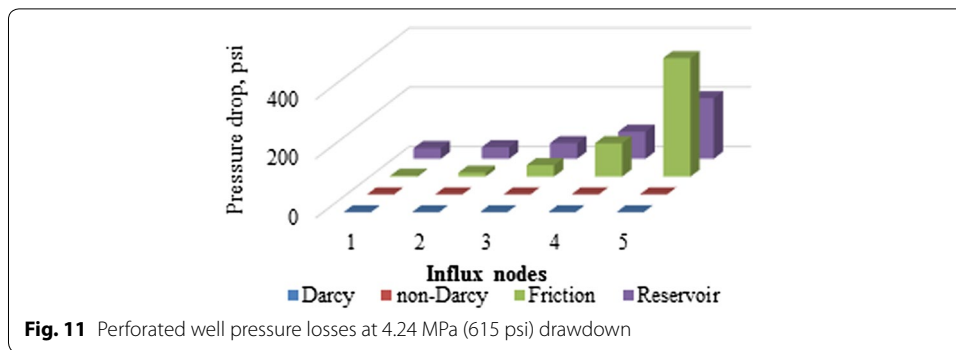


**Production side analysis**

**Case 1: unequal influx along the well**

The production side was simulated in order to understand the influx distribution along the well. Figure 10 illustrates the results for various well lengths with a constant pump drawdown pressure. As it is seen, the closest influx node to the brine pump location experiences the maximum value. Moving to the hill side the influx is reduced influencing frictional losses. The well length increase makes influxes more uneven. However, this has a negative effect on the heat transfer, due to uneven influx distribution along the pipe. As was expected, the frictional and reservoir pressure drops are the most valuable losses in the system (Fig. 11). More uniform influx distribution along the well has the shortest pipe of 150 m (457 ft) length.





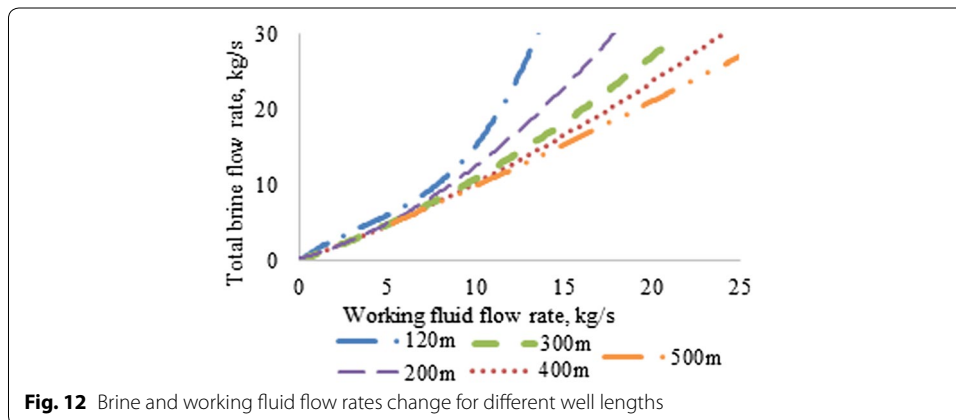
**Case 2: equal influx along the well (ICD case)**

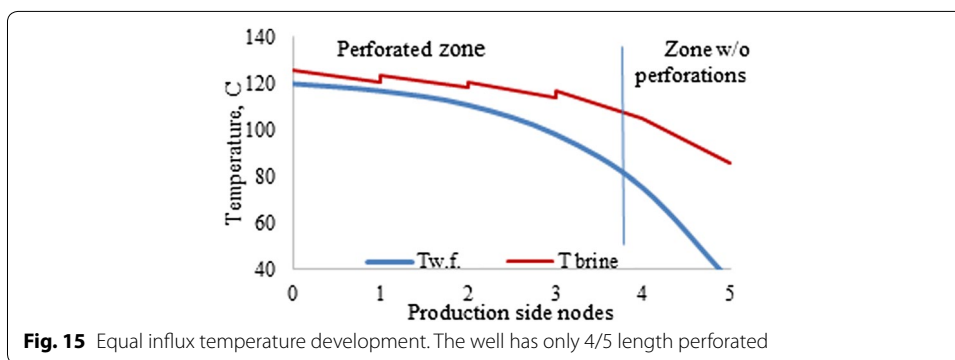
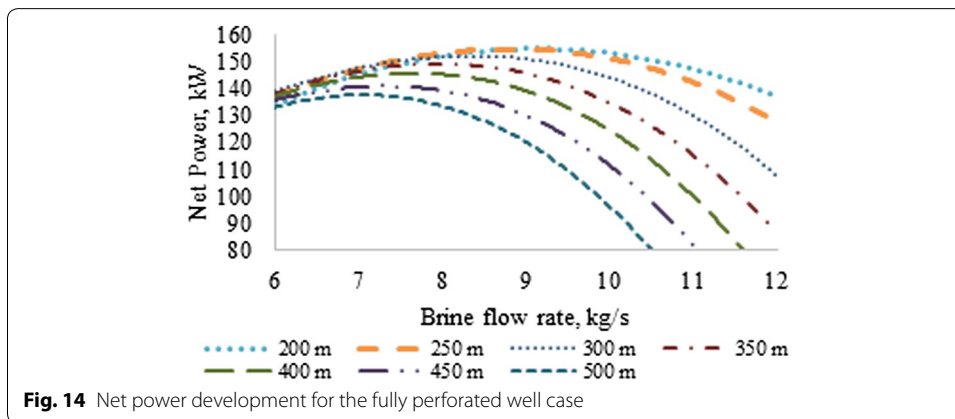
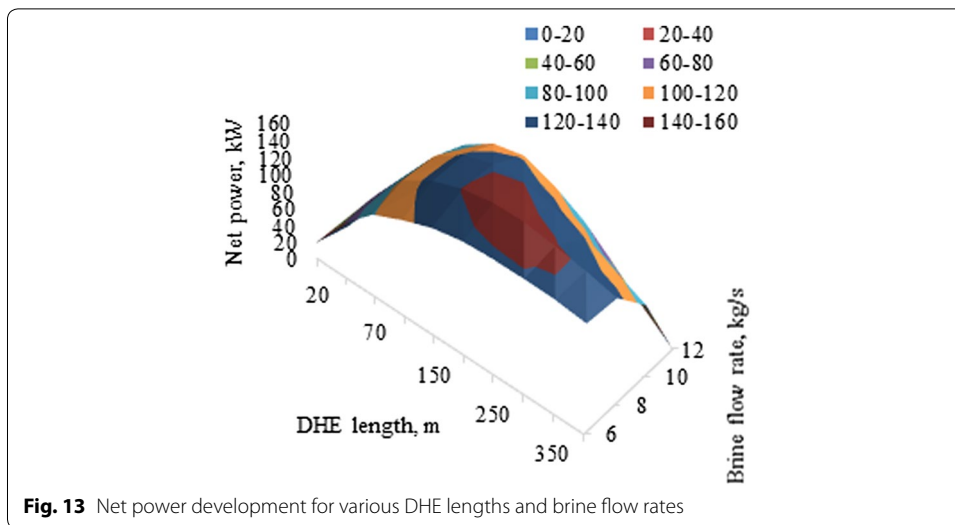
The influxes at each node were equalized by adding additional resistance to the gravel pack pressure drops at the nodes from #5 to #2. The #1 node pressure drop was kept constant and used as a reference. The system was iterated until all influxes would equalize. As it is seen from Fig. 12, the increase in length gives the more linear relationship between brine and working fluid flow rates.

To receive the maximum power, one would like to increase the working fluid flow rate. This requires higher heat transfer area. The DHE diameters are fixed by the well diameter constrain, so the length is the only parameter to change (Fig. 13). From the other side, length extension enhances frictional losses, so the produced net power drops after some optimal value (Figs. 13, 14). The maximum value of 160 kW was reached by the 200 m well at 10 kg/s brine flow rate matching 8.4 kg/s working fluid flow rate.

**Case 3: partially perforated well**

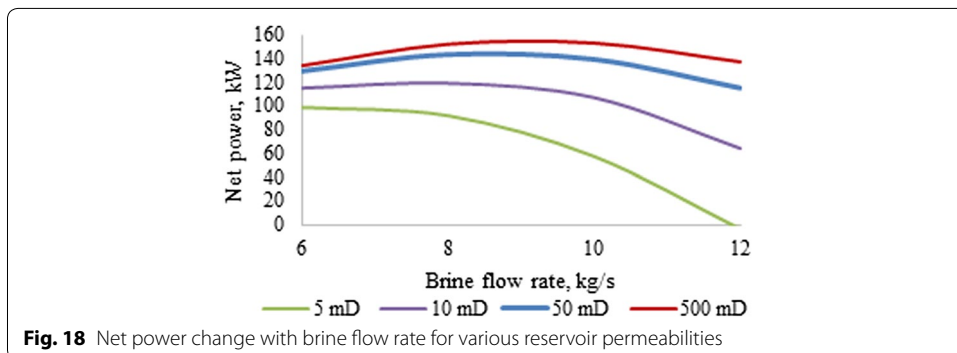
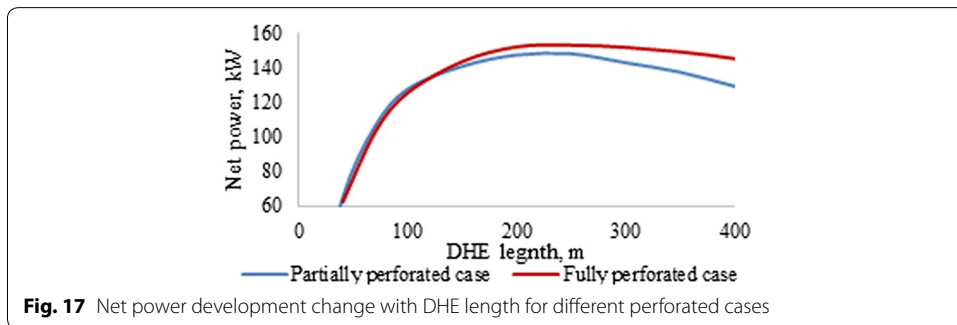
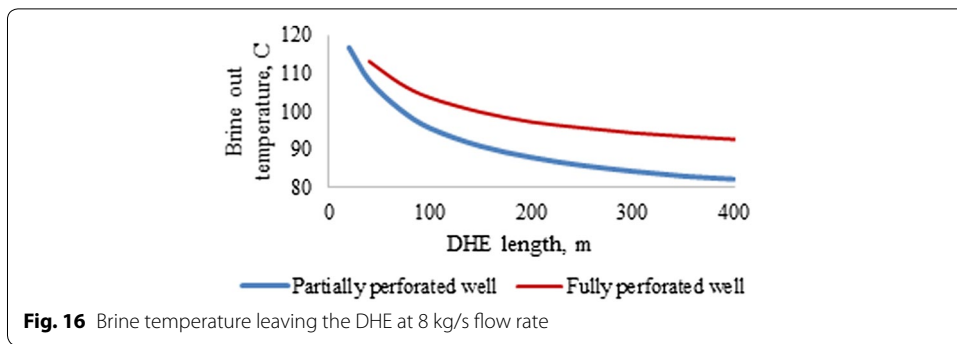
The well length can be perforated partially as shown in Fig. 15. The DHE is located in such way that the maximum brine influx matches with the coldest side of the working fluid stream. As a result, the brine temperature drops at the outlet of the DHE more than in the case of fully perforated production side (Fig. 16). In both cases, the 8 kg/s brine flow rate is the most power productive, however, fully perforated well has more net power delivery (Fig. 17).





**Case 4: permeability change**

Let us now simulate the system in terms of different reservoir permeabilities for various reservoir applications. The permeability reduction increases the reservoir flow resistance, while the internal well losses remain unchanged. With the same simulation conditions, the brine pump has the lowest load at the highest permeability (Fig. 18).

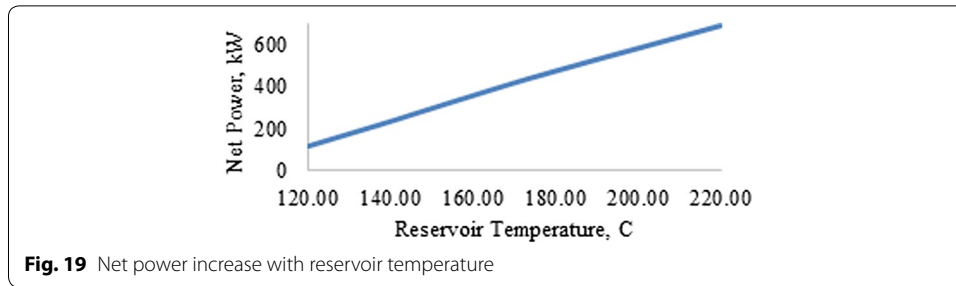


**Case 5: reservoirs with higher temperature**

Increasing reservoir temperature positively affects net power production. As it is seen in Fig. 19, the maximum net power of 600 kW can be reached at the 210 °C reservoir case.

**Completion design injection side**

The friction pressure drop inside the well is lower than that in the production side due to absent of the DHE inside the well. Thus, the well flowing pressures at the each node are very close to each other, and the outflux flow rates through the each perforation intervals are the same.



## Economics

### Methodology

The simplified model of the capital cost (CC) determination is defined by two major terms: drilling and completion cost (D&C) and power cycle cost (PC) (Walraven et al. 2015).

$$CC = D\&C + PC \quad (16)$$

The first term is subject to change due to the measured depth (MD) of the reservoir (Lukawski et al. 2014).

$$D\&C = 1.72 \times 10^{-7} \times MD^2 + 2.3 \times 10^{-3} \times MD - 0.62 \quad (17)$$

The power cycle equipment is separated into two groups: petroleum industry available parts and unique parts including turbine-generator assembly, and a condenser. The first group includes DHE, packers, and ESPs. Three retrievable packers are included into the design scheme as well as two ESPs. The costs of these units are much smaller than D&C and partially included into the capital cost adding 15% of contingency (Randebergi et al. 2012).

Condenser cost in \$ is defined from Smith (2005), including correction for chemical engineering (CE)-index of 620 in July 2013 for the air cooled condenser of area  $A_c$ . The CE-indices can be found in <http://www.che.com/pci/>:

$$CC_{\text{cond.}} = 1.67 \times 10^5 \left( \frac{A_c}{200} \right)^{0.89} 1.35 \left( \frac{650.9}{620} \right) \quad (18)$$

The heat transfer area  $A_c$  is determined from the heat transfer calculations assuming bare tube type with a diameter of 0.025 m (Incropera et al. 1990).

$$A_c = \frac{\dot{m}_{\text{wf}}(H_{\text{in}} - H_{\text{out}})_{\text{cond.}}}{UT_{\text{ln}}} \quad (19)$$

where  $(H_{\text{in}} - H_{\text{out}})_{\text{cond.}}$  is an enthalpy change of  $\text{CO}_2$  in the condenser;  $\dot{m}_{\text{wf}}$  is working fluid's mass flow rate; and  $U$  is overall heat transfer coefficient;  $T_{\text{ln}}$  log-mean temperature difference.

The turbine cost depends on turbine power produced and is defined from Walraven et al. (2015):

$$C_{\text{turb.}} = -1.66 \times 10^4 + 716 \times W_{\text{turb.}}^{0.8} \times 1.35 \quad (20)$$

The cost of power cycle parts:

$$C = CC_{\text{cond.}} + C_{\text{turb.}} \tag{21}$$

The obtained cost of power cycle parts is corrected for non-standard material ( $f_M = 1.7$ ) for stainless steel; high working pressure conditions ( $f_p = 1.5$ ), and installation expenses ( $f_i = 0.6$ ) (Smith 2005).

$$PC = C(f_M f_p + f_i) \tag{22}$$

The procedure of calculating the taxes is complicated, especially, if the well is going to be drilled not by the consumer itself. But assuming the fact that this type of power plant would be built for the internal company consumption, the LCOE can be obtained from the known capital cost of the power unit divided by the total amount of electricity produced during operational time in years.

$$LCOE = \frac{PC + \sum_{t=1}^{t=30} C_{O\&M}(1+i)^{-t}}{\sum_{t=1}^{t=30} (E(1+i)^{-t})} \tag{23}$$

where  $i$  is a discount rate;  $t$  is years of operation (30 years), and  $C_{O\&M}$  is operation and maintenance cost,  $E$  is total power produced during operational period.

$$C_{O\&M} = 0.025C_{\text{tot.}} \tag{24}$$

$$E = W_{\text{net}}N \tag{25}$$

where  $N$  is a number of full load hours per year, assumed of 95% (Walraven et al. 2015).

**Reference reservoir economics**

The example of D&C cost calculation is shown in Table 4. The 15% contingency was assumed for any unexpected outgoings. The constant net power production of 160 kW was assumed for a single lateral well. Total well cost is about \$17.5 mln, which is higher than in Kaiser (2016). The reason for this is a generalized trend of the curve in Eq. (17).

Kaiser (2016) analyzed LCOE by computing all costs for the particular drilling operation and assumed 200 kW net power, which is 25% higher than in this project. The PC cost calculation results are presented in Table 5.

Three cases were simulated for LCOE analysis. As it is seen from Fig. 20, the LCOE increases with depth of the reservoir, and with discount rate reduction. The purple line represents a single lateral well with 10% discount rate. The red and green lines are constructed for four lateral wells. The discount rate for the red line is 4%. The green line assumes no drilling cost, but only recompletion of an existing well for the power production case. If the D&C cost is ignored and only recompletion cost is assumed as 20% of

**Table 4 D&C cost calculation results for reference reservoir**

Well measured depth, m	Drilling and completion cost, mln \$	15% contingency, mln \$	Total well cost (DC), mln \$
5000	15.18	2.277	17.457



**Table 5 PC cost calculation example**

Working fluid mass flow rate, kg/s	Heat rejection, MW	Condenser area, m <sup>2</sup>	Condenser cost, mln \$	Turbine cost, mln \$	Power cycle cost corrected, mln \$
10	1.85	21.51	0.032	0.081	0.356

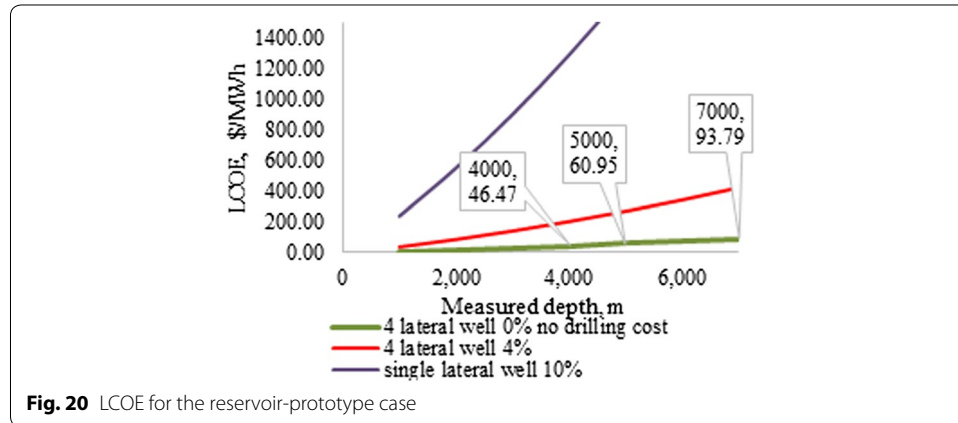


**Fig. 20** LCOE for the reservoir-prototype case

D&C cost, the \$46.47/MWh can be reached for 4000 m target depth reservoir with temperature of 126 °C. Note the DOE proposed LCOE for 2020 is \$48/MWh (By an MIT-led 2006; US Energy Information Administration 2017).

Increasing the net power (case with higher temperature reservoirs) plays crucial role in LCOE determination. For 220 °C reservoir temperature case, the red curve dropped the LCOE to less than \$100/MWh even for 7000 m depth (Fig. 21). The green line, representing recompletion case shows \$21.84/MWh at 7000 m TD, which is half than DOE requirements. In case of drilling and completion costs included into the account (red line), the increase in reservoir temperature gave optimistic shift toward satisfactory LCOE values (\$47.59/MWh at the 4 km TD). All simulations were done for carbon dioxide working fluid.

It is worth to note that not every petroleum well can be converted to the energy production unit for several reasons:

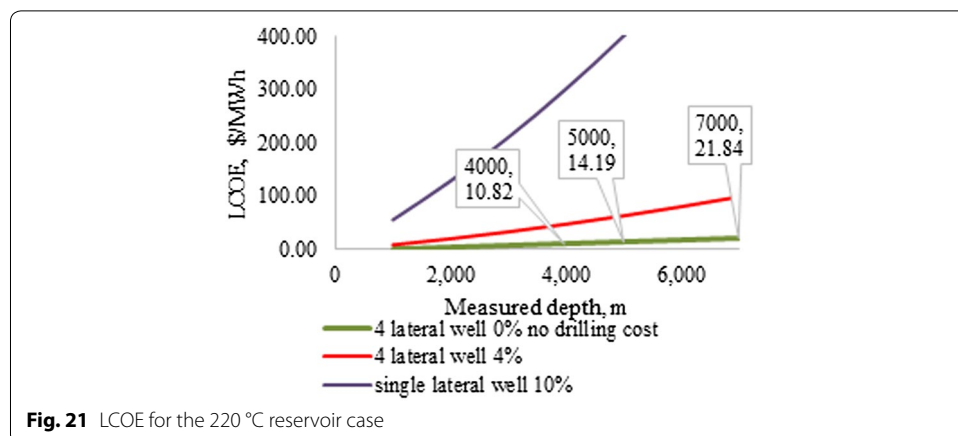


**Fig. 21** LCOE for the 220 °C reservoir case

- The well should have a horizontal section and a casing program should satisfy to the PC installation requirements. This includes inclination angles, perforated intervals, and casing diameters.
- The horizontal section should have enough diameter to install DHE in it. Very often the oil and gas wells have small diameters at the reservoir depth (less than 5 in.).
- The residual oil and gas content in the produced brine can cause several complications in reservoir circulation management. The temperature reduction in the DHE can provoke heavy fractions solidification and precipitation on the DHE part, which may cause clogging problems.

#### Risk assessment and cost:

- Before the petroleum well is drilled, the casing design and equipment should pass several standards and be certified. Adding energy production case to the petroleum project will eventually increase the cost of the well and add more standards.
- The petroleum well that served many years in production is not the same as new drilled well in terms of reliability and safety. It may require even more financial investment to transfer to the energy production unit. A detailed analysis may be a good topic for future exploration.

### Conclusions

The DHE analysis was performed for several cases. The optimization was performed for the maximum net power production.

- The optimal net power production depends on frictional losses inside the DHE. The optimal DHE length was found 200 m installed inside of 0.244 m (9 5/8 in. casing). Increasing the DHE length raises pressure losses in the horizontal well and, therefore, increases power spent on the brine pump.
- The scheme using ICD in the completion is preferable due to equalizing influxes along the well. ICD increases the working fluid flow rate and the total heat transferred to the power cycle.
- Perforated interval reduction is dropping the injection brine temperature and the net power production. Therefore, to receive the maximum power, the fully perforated well should be considered.
- The net power development is a function of brine flow rate, reservoir temperature, and frictional losses in the DHE. There is an optimal range where the maximum net power can be achieved.
- The injection side is designed with equal pressure losses principle and is free to change the perforation diameters, the number of shots, and perforated length. The injector does not have the DHE and a gravel pack completion. So, this side of the well is very adjustable to changes in production side and have equal out fluxes along the length.
- Higher permeability reservoir provides more net power due to less pressure resistance to flow and, therefore, less pumping requirement.

- Economic study shows that D&C cost is the most valuable for this project. The idea of recompletion of temporarily abandoned wells gives cheap electric power production for domestic usage with LCOE = \$48/MWh.
- With the application of DHE system to the higher enthalpy reservoirs, for example, 220 °C case, the LCOE drops down to \$21.84/MWh (7000 m depth) for recompletion case and stays less than \$100/MWh in the case of drilling the well at even for 7000 m depth reservoir.

### Future work

The distance between the production and injection sides was assumed according to work of Feng (2012). In fact, this interval is a function of brine outlet temperature, mass flow rate, reservoir permeability, and position of the well in the reservoir thickness. The increase in the interval creates additional drilling expenses, reduction threatens by producing cooler fluid than expected. The future work is dedicated to defining the minimum interval length with optimal brine flow rate in order to avoid an influx of cooled brine into the production side.

### Abbreviations

a1: annulus 1; a2: annulus 2; b: brine; b.p.: brine pump; cond.: condenser; e: belongs to reservoir; gen.: generator; gravel: gravel pack; in: inlet; out: outlet; Prod.: produced brine; perf.: perforations; sf: sand face; spf: shots per foot; tot. total; turb.: turbine; tub.: tubing; wf: working fluid; wf.p: working fluid pump.

### List of symbols

$L$ : length, m;  $k$ : permeability, mD;  $Q$ : flow rate through the one perforation  $\text{kg}/\text{m}^3$ ;  $B_b$ : formation volume factor, bbl.res/STB;  $P$ : pressure, Pa;  $t$ : operational time, years;  $\Delta l$ : perforated interval, m;  $C_p$ : specific heat,  $\text{kJ}/\text{kg}/\text{K}$ ;  $\dot{m}$ : mass flow rate,  $\text{kg}/\text{s}$ ;  $T$ : temperature, °C;  $R$ : thermal resistance,  $\text{W}/\text{K}$ ;  $H$ : enthalpy,  $\text{J}/\text{kg}$ .

### Greek letters

$\beta$ : permeability ratio;  $\theta$ : inclination angle, degrees;  $\emptyset$ : reservoir porosity;  $\mu$ : brine viscosity, cp;  $\rho$ : density,  $\text{kg}/\text{m}^3$ .

### Authors' contributions

IA wrote the simulator, performed all calculations, and wrote this manuscript. MT critically reviewed the manuscript and managed the project. Both authors read and approved the final manuscript.

### Acknowledgements

The authors gratefully acknowledge financial support for this work from the US Department of Energy under the Grant DE-EE0005125.

### Competing interests

The authors declare that they have no competing interests.

### Availability of data and materials

The dataset(s) supporting the conclusions of this article is (are) included within the article.

### Consent for publication

Not applicable.

### Ethics approval and consent to participate

Not applicable.

**Funding**

The project was performed under the financial support from the US Department of Energy under the Grant DE-EE0005125.

**Appendix A**

**Flow in reservoir**

The reservoir drainage area was assumed to have an elliptical shape as described by Joshi (1988).

Reservoir ellipse drainage flow can be described by:

$$P_e - P_{well} = \frac{\mu_b B_b \left[ \ln(X) + \frac{h\beta}{L} \ln\left(\frac{2\beta}{1+\beta} \frac{h}{2\pi r_w}\right) + S_H \right]}{2\pi k_c h \rho_b} \dot{m}_b \tag{26}$$

where  $B_b$  is geo-fluid productivity index,  $S$  is a perforations skin factor (Bellarby 2009),  $h$  is reservoir height,  $L$  is production or injection interval length,  $k_c$  is permeability of the damaged zone, and  $r_w$  is well radius.

Parameter  $X$  depends on shape of drainage area and with assumption of  $a > L$  can be found from:

$$X = \frac{a + \sqrt{a^2 - \left(\frac{L}{2}\right)^2}}{\frac{L}{2}} \tag{27}$$

$$a = \frac{L}{2} \sqrt{0.5 + \sqrt{0.25 + \left(\frac{2r_e}{L}\right)^4}} \tag{28}$$

where  $r_e$  is reservoir radius.

Damaged zone skin factor  $S_H$ :

$$S_H = \frac{h}{L} \left( \frac{k_h}{k_s} - 1 \right) \ln\left(\frac{r_s}{r_w}\right), \tag{29}$$

where damaged radius  $r_s$  can be obtained from logs Gray (2010),  $r_w$  is well radius,  $k_h$  is horizontal permeability. Permeability of damaged zone  $k_s$  can be formulated as:

$$k_s = 0.3474 \log\left(\frac{(P_e - P_{well})}{10^{-0.531 \log(k_h) + 2.2783}}\right) k_h \tag{30}$$

$$\beta = \sqrt{\frac{k_h}{k_v}} \tag{31}$$

Gravel pack model:

$$\Delta P_{gravel} = aQ^2 + bQ = \frac{\gamma B_b^2}{A_G^2 \rho_b} \dot{m}_b^2 + \frac{\mu_b B_b L_G}{A_G k_G \rho_b} \dot{m}_b \tag{32}$$

where  $A_G$ ,  $k_G$ ,  $L_G$  is area, permeability, and length of gravel pack.

The  $B_b$  term can be dropped because fluid does not get to the surface.

$$\gamma = \frac{1.47 * 10^7}{k_G^{0.55}} \quad (33)$$

$$A_G = A_{\text{perf}} \times (\text{spf}) \times L_{\text{perf}} \quad (34)$$

where the area of perforation is defined by shots per foot spf, diameter of perforations  $D_{\text{perf}}$  and perforated pipe segment length  $L_{\text{perf}}$ :

$$A_{\text{perf}} = \frac{\pi D_{\text{perf}}^2 \text{spf} L_{\text{perf}}}{4} \quad (35)$$

## Appendix B

### Flow in the pipe

Pressure change along the pipe with the assumption of inclination toward the pump:

$$\Delta P = F \dot{m}_{\text{in}}^2 + A \dot{m}_{\text{in}} - G \quad (36)$$

where

$$F = \frac{f_{\text{tot}} \Delta L}{2A_{\text{pipe}}^2 \rho_b D_h} \quad (37)$$

where  $\Delta L$  is interval between the nodes.

$$A = \frac{\dot{m}_{\text{tot}}}{A_{\text{pipe}} A_{\text{in}} \rho_b} \quad (38)$$

$$G = \rho_b g \Delta L \sin(\alpha) \quad (39)$$

where for flow in the annulus:

$$A_{\text{pipe}} = \frac{\pi (D_o^2 - D_i^2)}{4} \quad (40)$$

Total friction factor was calculated from Asheim (1992):

$$f_{\text{tot}} = f_{\text{wall}} + f_{\text{perf}} = 0.16 \text{Re}^{0.19} + 4D \frac{\dot{m}_{\text{in}}}{\dot{m}_{\text{tot}}} \quad (41)$$

The influx area  $A_{\text{in}}$  in a case of openhole or perforated wall without DHE can be defined as:

$$A_{\text{in}} = \pi D_o \Delta L \quad (42)$$

## Appendix C

### Heat transfer

Heat transfer process in the DHE was analyzed referring to Feng (2012). Brine is flowing through the annulus 2 and working fluid is entering to the DHE through the tubing and

leaving through the annulus 1. Thus, the flow rates in the tubing and annulus 1 are equal  $\dot{m}_t = \dot{m}_{a1}$ .

Insulated tubing temperature  $T_t$  is defined as temperature at the condenser exit  $T_{\text{cond.out}}$  and additional temperature gain at the pump stage  $\Delta T_{\text{wf,p}}$ :

$$T_t = T_{\text{cond.out}} + \Delta T_{\text{wf,p}} \tag{43}$$

Annulus 1:

$$Cp_{a1} \dot{m}_{a1} \frac{dT_{a1}}{d\Delta L} = \frac{T_{a2} - T_{a1}}{R_{a2/a1}} \tag{44}$$

Annulus 2:

$$Cp_{a2} \dot{m}_{a2} \frac{dT_{a2}}{d\Delta L} = \frac{T_e - T_{a2}}{R_{e/a2}} - \frac{T_{a2} - T_{a1}}{R_{a1/a2}} \tag{45}$$

where,  $Cp_{a1}$ ,  $Cp_{a2}$  are specific heats of the liquid flowing through the annuluses 1 and 2 respectively;  $\dot{m}_{a1}$ ,  $\dot{m}_{a2}$  are mass flow rates through annuluses 1, 2 respectively;  $T_{a1}$ ,  $T_{a2}$ ,  $T_e$ —are fluid temperatures in the annuluses 1, 2, and reservoir respectively;  $\Delta L$  is heat exchanger interval;  $R_{e/a2}$ ,  $R_{a2/a1}$ —are thermal resistances between reservoir and annulus 2, and annulus 2 and 1.

Initial conditions:

$$x = 0; T_{a1} = T_t; T_{a2} = T_e \tag{46}$$

Working fluid temperature flowing in the annulus 1 is obtained from Eq. (47) with  $j$ -direction flow:

$$T_{(j+1)\text{wf}} = T_{(j)\text{wf}} + \Delta L \frac{U_{(i)} (T_{(j)} + T_{(j-1)})_{\text{wf}}}{\dot{m}_{\text{wf}(j)} Cp_{\text{wf}(j)}} \tag{47}$$

Brine temperature flowing in the annulus 2 is obtained from Eq. (48) with  $i$ -direction flow opposite to the working fluid:

$$T_{(i+1)\text{b}} = T_{(i)\text{b}} - \Delta L \frac{U_{(i)} (T_{(i)} - T_{(i-1)})_{\text{b}}}{\dot{m}_{\text{b}(i)} Cp_{\text{b}(i)}} \tag{48}$$

Then brine temperature is updated at each node according to calculated influx:

$$T_{(\text{new})\text{b}} = T_{(\text{old})\text{b}} + \frac{\dot{m}_{\text{b}(i)}}{\dot{m}_{\text{b}(\text{tot})}} T_{(e)\text{b}} \tag{49}$$

The main interest of the work is designing a compact and efficient heat exchanger. The diameters are already specified, so the length is the only value to play with:

$$L_{\text{DHE}} = \frac{\dot{m}_{\text{b}(\text{tot})} Cp_{\text{b}} (T_{\text{in}} - T_{\text{out}})_{\text{b}}}{R_{a2/a1} \pi D_{a2,i} \Delta T_{\text{lm}}} \tag{50}$$

Thermal resistance between the reservoir rock and annulus 2  $R_{e/a2}$  is a sum of convective term  $R_{a2,conv}$  and conduction terms in the casing pipe  $R_{cas,cond}$  and cement sheath  $R_{cem,cond}$ .

$$R_{e/a2} = R_{a2,conv} + R_{cas,cond} + R_{cem,cond} \tag{51}$$

$$R_{a2,conv} = \frac{1}{\pi D_{a2,o} h_{a2}} \tag{52}$$

$$R_{cas,cond} = \frac{\ln\left(\frac{D_{cas}}{D_{a2}}\right)}{2\pi k_{cas}}$$

$$R_{cem,cond} = \frac{\ln\left(\frac{D_{cem}}{D_{cas}}\right)}{2\pi k_{cem}} \tag{53}$$

Thermal resistance between annulus 2 and annulus 1 consists of three components:

$$R_{an2/a1} = R_{a2,conv} + R_{pipe,cond} + R_{a1,conv} \tag{54}$$

$$R_{a2,conv} = \frac{1}{\pi D_{a2,i} h_{a2}} \tag{55}$$

$$R_{pipe,cond} = \frac{\ln\left(\frac{D_{a2,i}}{D_{a1,o}}\right)}{2\pi k_{pipe}} \tag{56}$$

$$R_{a1,conv} = \frac{1}{\pi D_{a1,i} h_{a1}} \tag{57}$$

Heat transfer coefficient for the annuluses:

$$h = \frac{Nuk}{D_o - D_i} \tag{58}$$

where the Nusselt number for laminar and turbulent flows is found from Eqs. (59) and (60) respectively:

$$Nu = 0.023Re^{0.8}Pr^n \tag{59}$$

where  $n = 0.4$  for heating and  $n = 0.3$  for cooling.

$$Nu = \frac{(f/8)(Re - 1000)Pr}{1 + 12.7\left(f/8\right)\left(Pr^{\frac{2}{3}} - 1\right)} \tag{60}$$

Reynolds  $Re$  and Prandtl numbers  $Pr$  are borrowed from Incropera et al. (1990).

## Publisher's Note

Springer Nature remains neutral with regard to jurisdictional claims in published maps and institutional affiliations.

Received: 17 April 2017 Accepted: 19 July 2017

Published online: 29 July 2017

## References

- Aadnoy B, Hareland G. Analysis of inflow control devices. 2009. doi:[10.2118/122824-MS](https://doi.org/10.2118/122824-MS).
- Akhdadullin I, Tyagi M. Design and analysis of electric power production unit for low enthalpy geothermal reservoir applications. *Int J Mech Mechatron Eng*. 2014;1:6.
- Al-Khelaiwi FT, Birchenko VM, Konopczynski MR, Davies DR. Advanced wells: a comprehensive approach to the selection between passive and active inflow-control completion. *SPE* 132976. 2008.
- Anklam E. Wellbore hydraulics. SPE-94316-MS, SPE production operations symposium, 16–19 April, Oklahoma City, Oklahoma. 2005.
- Asheim H, Kolnes J, Oudemans P. A flow resistance correlation for completed wellbore. *J Pet Sci Eng*. 1992;8(2):97–104.
- Bellarby J. Well completion design. *Developments in petroleum science*, vol. 56. New York: Elsevier Science; 2009. p. 639–642.
- Bourgoyne AT, Millheim KK, Chenevert K, Young FS. *Drilling engineering*, SPE textbook series, vol. 2. Society of Petroleum Engineers; 1986.
- By an MIT-led. Interdisciplinary panel (Chaired by JW Tester). The future of geothermal energy, impact of enhanced geothermal systems (EGS) on the United States in the 21st century. 2006.
- Cho H, Shah S. Prediction of specific productivity index for long horizontal wells. SPE 67237, SPE production and operations symposium, 25–27 March, Oklahoma City, Oklahoma. 2001.
- Dippippo R. *Geothermal power plants: principles, applications, case studies and environmental impact*. Oxford: Butterworth-Heinemann; 2008.
- Feng Y. Numerical study of downhole heat exchanger concept in geothermal energy extraction from saturated and fractured reservoirs. 2012. [http://digitalcommons.lsu.edu/gradschool\\_dissertations/53](http://digitalcommons.lsu.edu/gradschool_dissertations/53). Accessed 15 Aug 2012.
- Gray T. Geothermal resource assessment of the Gueydan salt dome and the adjacent southeast Gueydan field, Vermilion Parish, Louisiana. 2010. [http://digitalcommons.lsu.edu/gradschool\\_theses/299](http://digitalcommons.lsu.edu/gradschool_theses/299). Accessed 10 Dec 2014.
- Incropera F, DeWitt D, Lavine A. *Fundamentals of heat and mass transfer*. New York: Wiley; 1990.
- Joshi SD. Augmentation of well productivity with slant and horizontal wells. SPE-15375-PA, *J Pet Technol*. 1988;40:729–39.
- Kaiser M. Economic analysis of a zero-mass withdrawal geothermal energy system. *J Sustain Energy Eng*. 2016;3(3):191–220.
- Kubik M. The future of geothermal energy. Massachusetts Inst. of Technology (MIT), DOE report. 2006. ISBN: 0615134386.
- Lukawski MZ, Anderson BJ, Augustine C, Capuano LE, Beckers KF, Livesay B, Tester JW. Cost analysis of oil, gas, and geothermal well drilling. *J Pet Sci Eng*. 2014;118:1–14.
- Nalla G, Shook GM, Mines GL, Bloomfield K. Parametric sensitivity study of operating and design variables in wellbore heat exchangers. In: *Workshop on geothermal reservoir engineering*, Stanford University. 2004.
- Ouyang L, Arbabi S, Aziz K. General single phase wellbore flow model. DOE Report DE-FG22-93BC14862. 1997.
- Randebergi E, Fordi E, Nygaard G, Eriksson M, Gressgard L, Hanseni K. Potentials for cost reduction for geothermal well construction in view of various drilling technologies and automatization opportunities. In: *36th workshop on geothermal reservoir engineering*, Stanford University. SGP-TR-194. 2012.
- Sarkar J. Review and future trends of supercritical CO<sub>2</sub> Rankine cycle for low-grade heat conversion. *Renew Sustain Energy Rev*. 2015;48:434–51.
- Smith R. *Chemical process design and integration*. New York: Wiley; 2005.
- US Energy Information Administration. <https://www.eia.gov/electricity/monthly>. Accessed 20 Feb 2017.
- Walraven D, Laenen B, D'haeseleer W. Minimizing the levelized cost of electricity production from low temperature geothermal heat sources with ORCs: water or air cooled? *Appl Energy*. 2015;142:144–53.
- Wang Z, McClure M, Horne R. A single-well EGS configuration using a thermosiphon. In: *Workshop on geothermal reservoir engineering*, Stanford University, Stanford, CA. 2009.

Submit your manuscript to a SpringerOpen® journal and benefit from:

- Convenient online submission
- Rigorous peer review
- Open access: articles freely available online
- High visibility within the field
- Retaining the copyright to your article

Submit your next manuscript at ► [springeropen.com](http://springeropen.com)